Comprehensive characterization of mouse skin derived from regenerative versus reparative stages: a comparative analysis

Valentina Castillo[1], Pamela Díaz[2], Rocío Corrales-Orovio[1,3], Sebastián San Martín[2], José Tomás Egaña[1]
vfcastillo@uc.cl, jte@uc.cl

[1] Tissue Engineering and Regeneration Lab, Institute for Biological and Medical Engineering, Schools of Engineering, Biological Sciences and Medicine, Pontificia Universidad Católica de Chile, Santiago. [2] Universidad de Valparaiso, Biomedical Research Center, School of Medicine, Viña del Mar, Chile.[3] LMU, Division of Hand, Plastic and Aesthetic Surgery, Medicine, Munich, Germany

INTRODUCTION

Tissue regeneration capacities vary significantly in the course of life. For instance, some organism like mammals can fully regenerate only until determined fetal stages, after that tissue repairs take place without reestablish normal tissue architecture and function. The high regenerative potential of embryos has been attributed to several factors, such as stem cells, immune system, cell-response to specific growth factors, secretion of matrix-degrading proteases and the presence of particular extracellular matrix molecules upon damage. In order to contribute to better understand the changes that locally occurs in the transition between regenerative and reparative stages, in this work we carried out a comparative analysis between skin derived from mice at regenerative (E16.5) and reparative (6-8 weeks) stages.

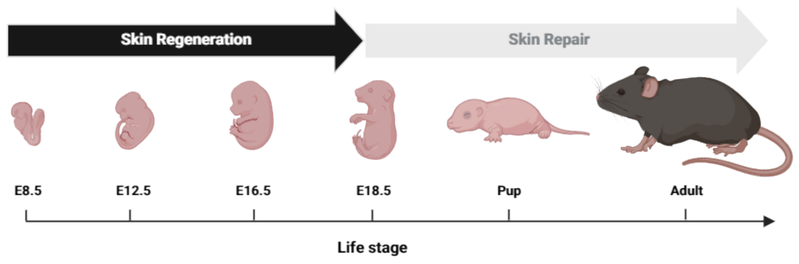

Figure 1. Regenerative potential of skin during mice development.

METHODS

Skin tissue derived from mice at regenerative (E16.5 fetus) and reparative (6-8 weeks old adult) stages was dissected and molecular, histological, structural, mechanical and functional analysis were performed.The molecular analysis included quantification of DNA, lipid and Sulfated Glycosaminoglycans (sGAGs) content, while histological analysis included stainning of fibrous proteins (collagens and elastin) and Carboxylated Glycosaminoglycans (cGAGs).The structural analysis was done throught scanning electron microscopy to quantify pore size and fibers thickness. Finally, as part of functional and mechanical characterization, metabolic activity, fluid capacity and Young modulus were quantified too.

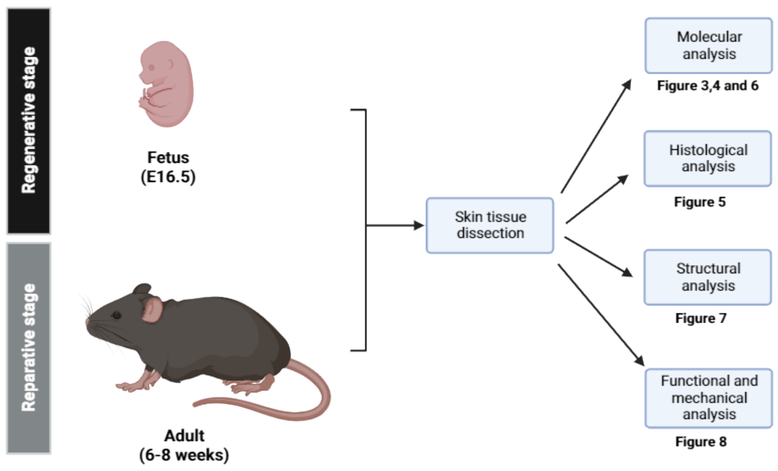

Figure 2. Experimental approach.

CONCLUSION

Here, we found that fetal skin composition differs not only in their molecular composition and distribution but also in their structure and functionality. Our results showed increased nuclei acid, collagen III and glycosaminoglycans content in regenerative versus reparative stages, while, differential lipid distribution, pore size and proteoglycans amount were observed too. Moreover, we also found that regenerative skin has significantly higher porosity, metabolic activity, fluid capacity and elasticity than reparative skin. This work provides a great knowledge about molecular, structural and functional hallmarks of skin derived from stages with regenerative abilities. Moreover, our results give insights for the development of new scaffolds with clinical potential able to mimic both structure and composition here described.

RESULTS

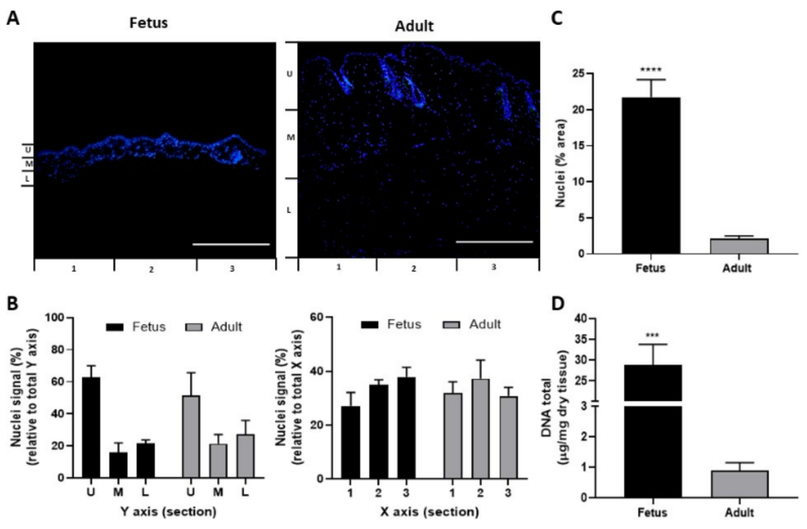

Figure 3. Nuclei distribution and DNA content of skin from fetus and adult mice. **(A)** Transversal skin cryosections stained with Hoechst nuclear probe. **(B)** Distribution of nuclei signal (%) relative to total Y axis (left) and total X axis (right). **(C)** Area covered by nuclei (%) relative total skin. **(D)** Spectrophotometric quantification of total dsDNA content relative to dry weight of tissue.

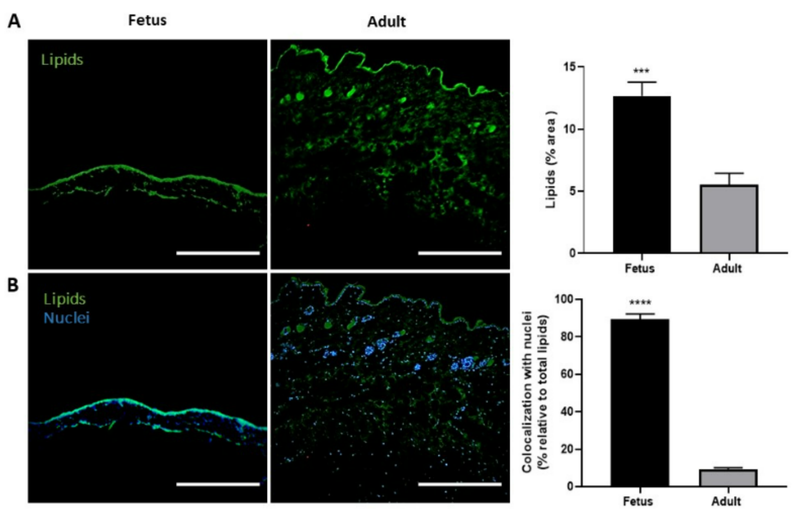

Figure 4. Lipids content and distribution of the skin from fetus and adult mice. **(A)** Transversal skin cryosections stained with BODIPY 493/503 probe showing neutral lipid (left) and quantification of area (%) covered by neutral lipids relative to total skin. **(B)** Transversal skin cryosections stained with BODIPY 493/503 and Hoechst stain showing neutral lipid overlapping with nuclei (left) and quantification of the percentage of lipids signal that colocalize with nuclei (right).

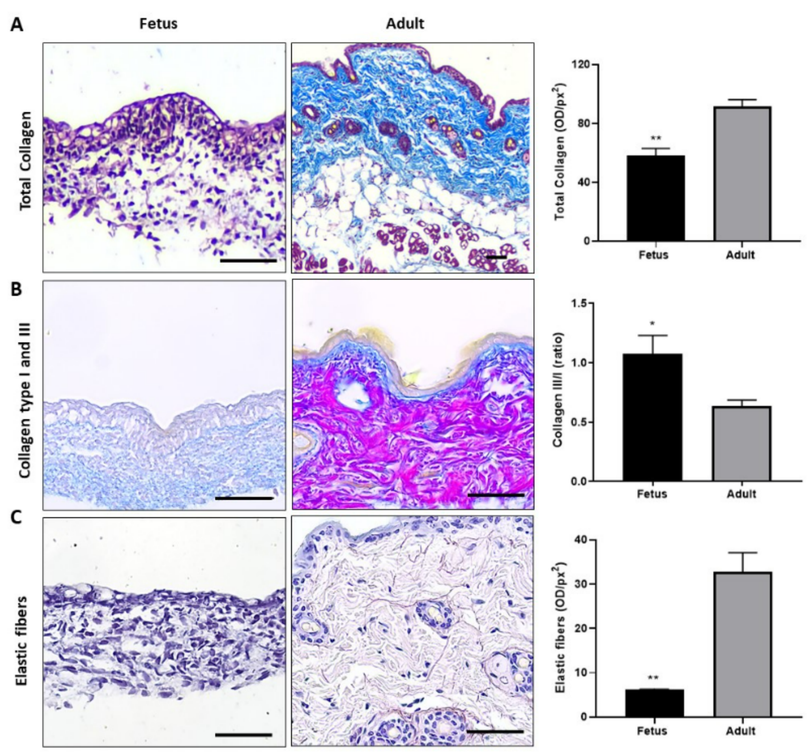

Figure 5. Fibrous protein content of extracellular matrix (ECM) of the skin from fetus and adult mice. Transversal paraffin skin sections stained with **(A)** Hematoxylin-Eosin stain (left) and its densitometric analysis (right) reported as optical density (OD)/px^2. **(B)** Herovici Collagen stain (left) showing collagen I (pink) and III (blue) together with collagen III/I ratio plot (right) obtained from densitometric analysis of both type of collagen (data not shown). **(C)** Orcein Elastic fibers stain (left) and its densitometric analysis (right) reported as optical density/pixeles^2 (OD/px^2).

RESULTS

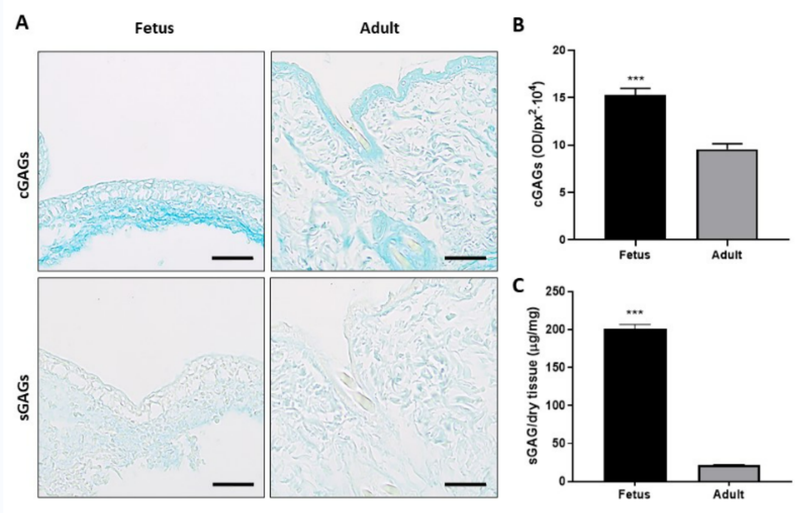

Figure 6. Glycosaminoglycans (GAGs) content of skin from fetus and adult mice. **(A)** Carboxylated Glycosaminoglycans (cGAGs) stain with Alcian blue pH 2.5 (Top) and Sulfated Glycosaminoglycans (sGAGs) stain with Alcian blue pH 1.0 (Bottom). **(B)** cGAGs optical density (OD/px2) and **(C)** sGAGs quantification (µg/mg dry tissue) by Blyscan ™ assay.

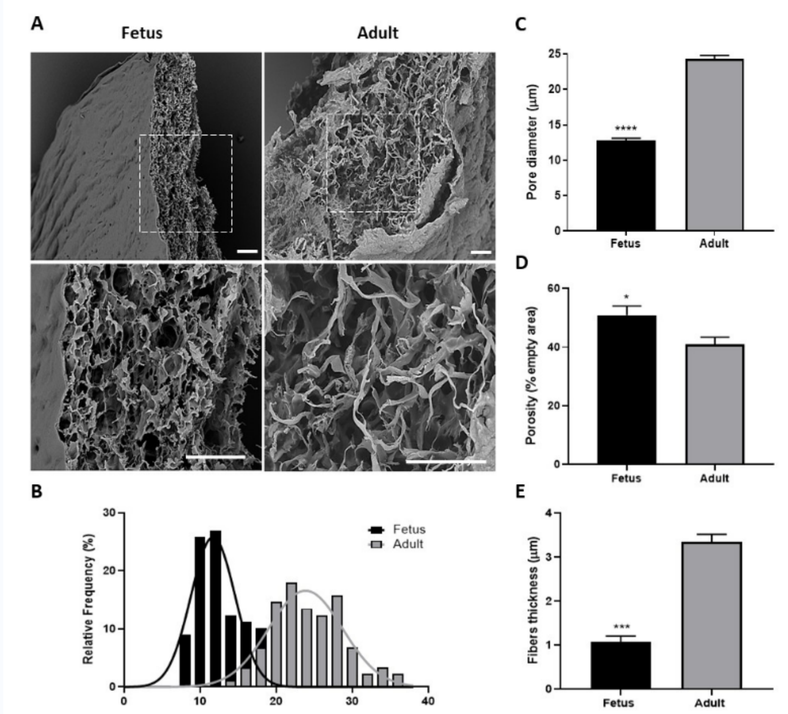

Figure 7. Ultrastructural comparison between skin from fetus and adult mice. **(A)** Scanning electron microscopy (SEM) of skin from fetus and adult mice. **(B)** Pore diameter distribution of skin from fetus and adult mice shown as relative frequency (%). **(C)** Mean pore diameter (µm). **(D)** Porosity shown as percentage of empty area. **(E)** Mean fibers thickness (µm).

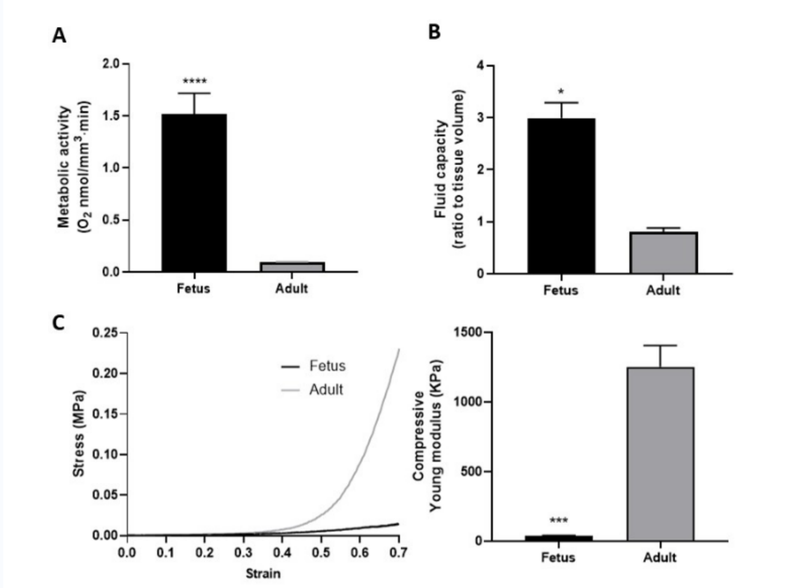

Figure 8. Metabolic and functional comparison between skin from fetus and adult mice. **(A)** Metabolic activity quantification by oxygen consumption normalized by tissue volume. **(B)** Fluid capacity as indicative of water absorption capability quantified relative to tissue volume. **(C)** Compressive Stress-strain curves (left) and Young Modulus (Kpa) quantification (right).

Funding

FONDECYT Regular 1200280-ANID